145 (2023) 213268

Contents lists available at ScienceDirect

Biomaterials Advances

journal homepage: www.journals.elsevier.com/materials-science-and-engineering-c

# Metal-organic framework for biomimetic nitric oxide generation and anticancer drug delivery

Han Bi Ji [a,1], Se-Na Kim [b,1], Cho Rim Kim [a], Chang Hee Min [a], Jae Hoon Han [a], Min Ji Kim [a], Cheol Lee [c], Young Bin Choy [a,b,d,*]

[a] Interdisciplinary Program in Bioengineering, College of Engineering, Seoul National University, Seoul 08826, Republic of Korea
[b] Institute of Medical & Biological Engineering, Medical Research Center, Seoul National University, Seoul 03080, Republic of Korea
[c] Department of Pathology, Seoul National University College of Medicine, Seoul 03080, Republic of Korea
[d] Department of Biomedical Engineering, Seoul National University College of Medicine, Seoul 03080, Republic of Korea

ARTICLE INFO

*Keywords:*
Multidrug resistance cancer
Metal-organic framework
Nitric oxide
Sustained drug delivery

ABSTRACT

The potential therapeutic implications of nitric oxide (NO) have drawn a great deal of interest for reversing multidrug resistance (MDR) in cancer; however, previous strategies utilized unstable or toxic NO donors often oxidized by the excessive addition of reactive oxygen species, leading to unexpected side effects. Therefore, this study proposed a metal-organic framework (MOF), Porous coordination network (PCN)-223-Fe, to be loaded with a biocompatible NO donor, L-arginine (L-arg; i.e., PCN-223-Fe/L-arg). This specific MOF possesses a ligand of Fe-porphyrin, a biomimetic catalyst. Thus, with PCN-223-Fe/L-arg, L-arg was released in a sustained manner, which generated NO by a catalytic reaction between L-arg and Fe-porphyrin in PCN-223-Fe. Through this biomimetic process, PCN-223-Fe/L-arg could generate sufficient NO to reverse MDR at the expense of hydrogen peroxide already present and highly expressed in cancer environments. For treatment of MDR cancer, this study also proposed PCN-223-Fe loaded with an anticancer drug, irinotecan (CPT-11; i.e., PCN-223-Fe/CPT-11), to be formulated together with PCN-223-Fe/L-arg. Owing to the synergistic effect of reversed MDR by NO generation and sustained release of CPT-11, this combined formulation exhibited a higher anticancer effect on MDR cancer cells (MCF-7/ADR). When intratumorally injected in vivo, coadministration of PCN-223-Fe/L-arg and PCN-223-Fe/CPT-11 greatly suppressed tumor growth in nude mice bearing MDR tumors.

## 1. Introduction

Cancer is one of the leading causes of deaths worldwide [1]. Treatment of ~50 % of cancer includes chemotherapy [2]. However, the effectiveness is often limited by tumor cells expressing the multidrug resistance (MDR) phenotype [3]. MDR is the phenomenon by which tumor cells that have been exposed to a single cytotoxic agent develop cross-resistance to other structurally and functionally unrelated classes of cytotoxic agent [4,5]. The development of MDR is often related to the overexpression of efflux pumps located in the cell membrane, such as P-glycoprotein (P-gp), which is responsible for pumping out exogenous materials from cells [6–8]. The overexpression of these pumps prevents the sufficient accumulation of anticancer drugs within the tumor cell, resulting in limited therapeutic effectiveness [9]. This mechanism allows tumors to evade chemotherapy, so MDR remains one of the major clinical obstacles in tumor treatment [10,11].

Nitric oxide (NO) is a vital endogenous gaseous mediator that participates in various physiological and biological pathways [12–14]. In recent years, NO has been reported to play an important role in reversing MDR effects by downregulating P-gp expression levels [15–17]. Owing to this effect, the combined delivery of NO and an anticancer drug is considered a promising strategy for improving chemotherapeutic effects [18–20]. However, the gaseous phase and short half-life (3–4 s) and the high reactivity to biological substances have limited the direct application of NO [21,22]. For this reason, small-molecule NO donors, such as diethylenetriamine, diazeniumdiolate, and S-nitrosothiol, have been employed with microcarrier or nanocarrier systems, from which NO can be generated under various stimuli, such as pH, light and ultrasound, and metal catalysts [23–26]. Although many of these systems have shown potential in overcoming MDR with improved chemotherapeutic

* Corresponding author at: Department of Biomedical Engineering, Seoul National University College of Medicine, Seoul 03080, Republic of Korea.
*E-mail address:* ybchoy@snu.ac.kr (Y.B. Choy).
[1] These authors contributed equally as first authors to the work.

https://doi.org/10.1016/j.bioadv.2022.213268
Received 14 September 2022; Received in revised form 12 December 2022; Accepted 19 December 2022
Available online 23 December 2022

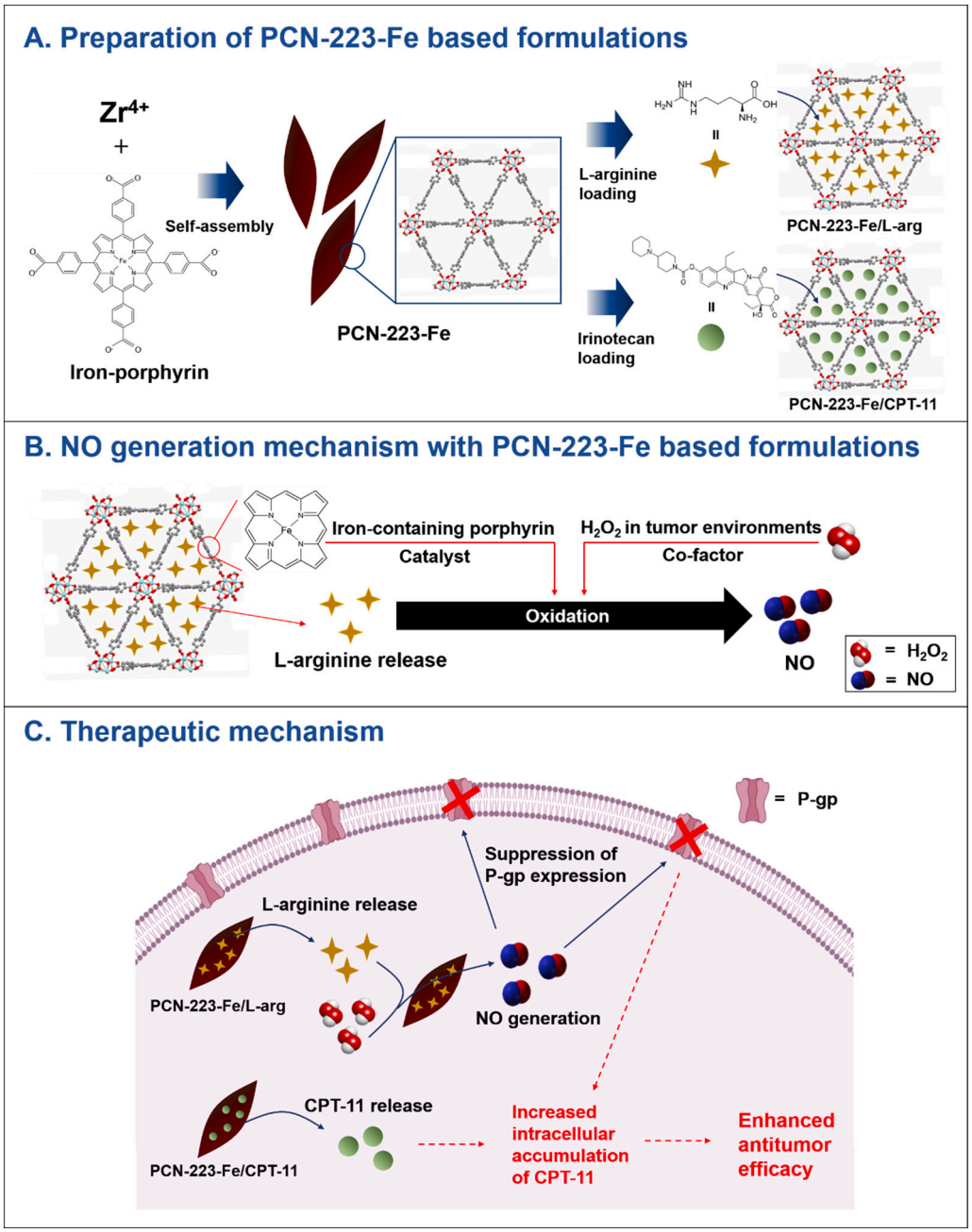


**Scheme 1.** Schematic description of PCN-223-Fe-based formulations. (A) Fabrication of PCN-223-Fe/L-arg and PCN-223-Fe/CPT-11. (B) Mechanism of NO generation from PCN-223-Fe/L-arg. (C) Therapeutic strategy for MDR cancer treated with a combined formulation of PCN-223-Fe/L-arg and PCN-223-Fe/CPT-11.

response, those NO donors often require a complex design of formulations due to low aqueous stability and lack of tumor specificity [27,28]. Moreover, after generating NO, these molecules are degraded into carcinogenic or proinflammatory byproducts, leading to unexpected side effects in normal, healthy cells [29,30].

Arginine has been proposed as an NO donor with excellent biocompatibility [31,32]. This naturally occurring compound, when oxidized, generates NO with a nontoxic byproduct of citrulline [33,34]. Thus, to the authors' knowledge, previous strategies of NO generation have focused mostly on the direct application of reactive oxygen species (ROS), such as hydrogen peroxide ($H_2O_2$) and hydroxyl radicals, to oxidize arginine [35,36]. For example, glucose oxidase was delivered together to oxidize glucose and produce $H_2O_2$ [35]. In this reaction, however, endogenous oxygen was essential as a precursor; thus, the efficiency of $H_2O_2$ generation was limited by the tumor's hypoxic environment [37]. Therefore, to be more effective, a higher ROS production can be advantageous; however, when excessive, ROS may cause oxidative stress and damage to cellular components in the surrounding normal tissue [38,39].

Therefore, this study proposed a formulation of a metal-organic framework (MOF), porous coordination network (PCN)-223-Fe, loaded with L-arginine (L-arg) as a novel means of NO generation (Scheme 1 (A)). PCN-223-Fe is composed of biocompatible constituent materials: a metal cluster of zirconium (Zr) and an organic ligand, Fe-containing porphyrin (Fe-porphyrin) [40,41]. As a porous crystalline material [42], PCN-223-Fe can work as a carrier for the sustained release of L-arg (i.e., PCN-223-Fe/L-arg) [43]. More importantly, this specific ligand of PCN-223-Fe possesses a structure of hemoprotein known to exhibit the function of NO synthase (NOS) in the human body [44]. The ligand as a Fe-porphyrin catalyst would react with endogenous $H_2O_2$ in tumor cells

to form an active high-valent iron-oxo complex, which is a key reactive intermediate in the catalytic cycle and has a strong oxidizing ability [45]. Therefore, through this process, L-arg released from PCN-223-Fe/L-arg would be oxidized to effectively produce NO at the expense of $H_2O_2$, the level of which is known to be already sufficiently high in tumor environments (5 μM–1 mM; Scheme 1(B)) [46,47]. This mechanism is based on the oxidative transformation of endogenous molecules being orchestrated by the biomimetic catalyst and NO donor; hence, there is no need for an additional ROS [48].

Therefore, this study ultimately proposed a formulation of PCN-223-Fe/L-arg combined with PCN-223-Fe loaded with an anticancer drug, irinotecan (CPT-11; i.e., PCN-223-Fe/CPT-11; Scheme 1(A)). When delivered in MDR tumor cells, this entity would generate NO through a biomimetic process and release the anticancer drug in a sustained manner, which would increase the intracellular accumulation of the drug by reversing the MDR effect, thereby improving chemotherapeutic efficacy (Scheme 1(C)). This formulation was first tested in in vitro environments to examine the property of NO generation and sustained drug release. In vitro efficacy was also evaluated using MCF-7/ADR breast cancer cells. This study evaluated the in vivo performance of a xenograft model of MCF-7/ADR in nude mice, where the formulation was administered via intratumoral injections [49,50].

## 2. Materials and methods

### 2.1. Materials

Zirconium chloride ($ZrCl_4$; >99.9 %), dimethylformamide (DMF; anhydrous; 99.8 %), benzoic acid (>99.5 %), L-arg (>98 %), sodium nitrate (99 %), phosphoric acid (85 %), formic acid (>98 %), formalin (neutral buffered; 10 %), nitrate reductase, and NADPH (97 %) were obtained from Sigma-Aldrich (St. Louis, MO, USA). Fe(III) meso-tetra(4-carboxyphenyl)porphyrin chloride (Fe-TCPP; >95 %) and CPT-11 (>99 %) were purchased from Combi-Blocks (San Diego, CA, USA) and LC Laboratories (Woburn, MA, USA), respectively. Acetonitrile (ACN; 99.9 %) and 2,3-diaminonaphthalene (DAN; >98 %) were purchased from J. T. Bakers (Pittsburgh, PA, USA) and TCI (Chuo-ku, Japan), respectively. Ethanol (>96 %), ammonium acetate (98 %), and $H_2O_2$ (30 %–35 %) were obtained from Daejung Chemicals (Siheung, Korea). Hydrochloric acid (HCl; 35 %) was purchased from Samchun Chemicals (Seoul, Korea). PBS (pH 7.4) and Dulbecco's modified Eagle's medium were purchased from Seoul National University Biomedical Research Institute (Seoul, Korea) and Welgene (Gyeongsan, Korea), respectively. Fetal bovine serum (FBS) and penicillin-streptomycin (10,000 U/mL) were obtained from Thermo Fisher Scientific (Waltham, MA, USA). MCF-7/ADR cells were generously provided by the laboratory of Prof. In Kyu Park (Chonnam National University, Gwangju, Korea).

### 2.2. Preparation of PCN-223-Fe and its formulation

PCN-223-Fe was synthesized following a previously reported protocol with slight modifications [51]. Briefly, Fe-TCPP (100 mg, 0.113 mmol) and benzoic acid (2500 mg, 22.3 mmol) were dissolved in 15 mL DMF, to which a solution of $ZrCl_4$ (100 mg, 0.239 mmol) prepared in 5 ml DMF was subsequently added. The resulting mixture was vigorously stirred for 30 min and kept in an oven at 120 °C for 48 h. The solid brown product was collected and washed with DMF and ethanol to remove excess reactants, followed by drying at 80 °C for 6 h. Subsequently, the collected product was treated in a vacuum oven at 150 °C for 12 h to remove any residual solvent.

To prepare PCN-223-Fe/L-arg, 200 mg L-arg was first dissolved in 10 ml deionized (DI) water. To this solution, 100 mg dehydrated PCN-223-Fe was added while continuously agitated at 100 rpm for 48 h. The resulting suspension was filtered with a 200 nm nylon membrane filter (Hyundai Micro, Seoul, Korea) to obtain PCN-223-Fe/L-arg, washed with ethanol thrice, and dried at 70 °C. To prepare PCN-223-Fe/CPT-11, 50 mg CTP-11 was dissolved in 50 ml DI water, to which 50 mg dehydrated PCN-223-Fe was added while being continuously agitated at 100 rpm for 48 h. The resulting suspension was filtered using a 200 nm nylon membrane filter, washed with ethanol thrice, and dried at 70 °C.

### 2.3. Characterization

The powder XRD (PXRD) patterns of PCN-223-Fe, PCN-223-Fe/L-arg, and PCN-223-Fe/CPT-11 were obtained using an X-ray diffractometer (SmartLab, Rigaku, Japan) at 3 kW with CuKα radiation. The FTIR spectra of PCN-223-Fe, L-arg, PCN-223-Fe/L-arg, CPT-11, and PCN-223-Fe/CPT-11 were obtained using a TENSOR27 spectrophotometer (Bruker, Billerica, MA, USA) over the range of 4000 to 400 $cm^{-1}$ with a 4 $cm^{-1}$ resolution at room temperature. The surface area, pore size, and pore volume were determined by a surface area and porosity analyzer (BELSOPR-mini II, Microtrac-Bel, Osaka, Japan) at −196 °C. Before the measurements, the samples were degassed at 120 °C for 12 h under a vacuum. The hydrodynamic size and zeta potential were measured by dynamic light scattering (Zetasizer Nano ZS90, Malvern Panalytical, Malvern, UK). The size and morphology of PCN-223-Fe, PCN-223-Fe/L-arg, and PCN-223-Fe/CPT-11 were assessed by SEM (JEOL-7800F, JEOL, Tokyo, Japan) and TEM (JEM-2100, JEOL).

To measure the amount of encapsulated L-arg or CPT-11, 5 mg PCN-223-Fe/L-arg or PCN-223-Fe/CPT-11 was suspended in 50 ml DI water and agitated at 100 rpm at 37 °C for 2 days to fully extract the encapsulated compound. The suspension was centrifuged at 5000 rpm, where the supernatant was acquired and analyzed by high-performance liquid chromatography/mass spectrometry (HPLC/MS; Agilent 6120 Quadrupole LCMS Systems; Agilent Technologies, Santa Clara, CA, USA) equipped with a Diamonsil C18 column (4.6 × 150 mm, 5 μm pore; Dikma, Lake Forest, CA, USA). For L-arg analysis, a mobile phase composed of ACN and 0.1 % formic acid (70:30, v/v) was fed at 0.5 ml/min. The injection volume and the selective ion monitoring (SIM) of L-arg were set at 10 μl and 175 *m/z*, respectively [52]. For CPT-11 analysis, the mobile phase was prepared by mixing methanol and 10 mM ammonium acetate (80:20, v/v) and fed at 0.5 ml/min. The injection volume and ultraviolet (UV) absorbance were set at 10 μl and 360 nm, respectively. The SIM ion of CPT-11 was 587 *m/z* [53].

### 2.4. In vitro study on compound release and NO generation

To examine the release profile of L-arg, 5 mg PCN-223-Fe/L-arg was dispersed in 1 ml PBS (pH 5.5) in a dialysis bag (3.5 kDa MWCO; SnakeSkin Dialysis Tubing; Thermo Fisher Scientific) and immersed in 5 ml PBS (pH 5.5). The resulting medium was incubated at 37 °C under 100 rpm agitation in a shaking incubator (SI-600R; Jeio Tech, Daejeon, Korea). At scheduled times, 1 ml of the supernatant was extracted, and an equal volume of fresh medium was added back. The sampled medium was assessed by HPLC/MS as described above to measure the L-arg concentration. To examine the release profile of CPT-11, 3 mg PCN-223-Fe/CPT-11 was dispersed in 5 ml PBS (pH 5.5) in a dialysis bag (3.5 kDa MWCO; SnakeSkin Dialysis Tubing; Thermo Fisher Scientific) and immersed in 20 ml PBS (pH 5.5). The resulting medium was incubated at 37 °C under 125 rpm agitation in a shaking incubator (SI-600R; Jeio Tech). At scheduled times, 5 ml of the supernatant was collected, and an equal volume of fresh medium was added back. The sampled medium was assessed by HPLC/MS as described above to measure the CPT-11 concentration.

The amount of NO generated by L-arg, PCN-223-Fe, and PCN-223-Fe/L-arg was assessed by the 2,3-diaminonaphthalene-2,3-naphthyltriazole assay method with slight modifications [54,55]. Briefly, 1.25 mg L-arg, 3.75 mg PCN-223-Fe, or 5 mg PCN-223-Fe/L-arg, containing an equivalent amount of L-arg or PCN-223-Fe, was added to 1 ml PBS (pH 5.5) containing varying amounts of $H_2O_2$ (i.e., 1, 0.1, 0.01, and 0 mM $H_2O_2$) in a dialysis bag, respectively. After that, each dialysis bag was immersed in 5 ml of the same type of medium and incubated at 37 °C

under 100 rpm agitation in a shaking incubator. At scheduled times, 1 ml of the supernatant was extracted, and an equal volume of fresh medium was added back. Then, 30 μl of the extracted sample were mixed with 40 μl nitrate reductase (1 unit/ml) and 50 μl NADPH (120 μM) and incubated at 25 °C for 1 h to enzymatically convert nitrate to nitrite. After that, a nitrate-derived nitrite solution was incubated with 50 μl DAN solution (500 μM in 0.5 M HCl) at 25 °C, to which 50 μl NaOH solution (1.4 M) was added to quench the reaction and produce NAT, a NO-derived fluorescent product. The amount of NAT was measured by HPLC/MS with a mobile phase composed of a mixture of ACN and 0.1 % formic acid (50:50, v/v). The injection volume and flow rate were set at 20 μl and 0.5 ml/min, respectively. The SIM ion was 159 *m/z* [54].

### 2.5. Assessment of intracellular uptake

To examine the intracellular uptake profile, PCN-223-Fe was loaded with calcein, a fluorescent molecule [56,57]. For this, 50 mg PCN-223-Fe was added to 10 ml calcein solution (5 mg/ml) prepared in methanol and stirred at 100 rpm for 48 h. The resulting suspension was filtered using a 200 nm nylon membrane filter, washed with ethanol, and dried at 70 °C.

MCF-7/ADR cells were seeded onto a six-well plate at $10^6$ cells/well and incubated for 24 h at 37 °C with 5 % $CO_2$. Subsequently, the culture medium was replaced with 2 ml calcein-loaded PCN-223-Fe suspension at varying concentrations (0.1, 0.25, 0.5, and 1 mg/ml). After incubation for 0.5, 1, and 2 h, the well was thoroughly washed with PBS containing 1 % FBS to remove any calcein-loaded PCN-223-Fe still suspended in the medium. Then, 2 ml trypsin was added to each well and incubated for 5 min to detach the adherent cells. Subsequently, the cell suspension was centrifuged for 3 min at 1200 rpm, and the collected cells were suspended in 500 μl PBS and analyzed with a flow cytometer (FACSymphony™ A5; BD Biosciences, Franklin Lakes, NJ, USA). The analysis was performed using BD FACSDiva™ 8.0 software.

### 2.6. Assessment of NO generation in cells

To examine the degree of NO generation in cells, an NO probe, DAF-DA, was used to stain cells after treatment [20]. Briefly, MCF-7/ADR cells were seeded in six-well plates at a density of $10^6$ cells/well and cultured for 24 h. Afterward, 250 μg L-arg, 750 μg PCN-223-Fe, or 1 mg PCN-223-Fe/L-arg, containing an equivalent amount of L-arg or PCN-223-Fe, was added to 2 ml of the medium, which was added into the well and incubated for 24 h. Cells were washed with the culture medium several times and dyed with DAF-DA (10 μM) for 30 min. Cross-sections of the stained cells were imaged at 40× magnification with a confocal laser scanning microscope (CLSM; TCS SP8 STED CW; Leica Microsystems, Wetzlar, Germany) under excitation and emission wavelengths at 488 and 515 nm, respectively. For each treatment, four experiments were performed to obtain four distinct images, which were assessed using ImageJ (NIH, Maryland, USA) for quantitative analysis. In each image, a region showing a fluorescent signal was selected, where an average value of fluorescence intensity was obtained by dividing a total sum of intensity values by the total selected area. The value of treated cells was then displayed as a relative fluorescence based on that of cells without treatment.

### 2.7. In vitro cytotoxicity evaluation

In vitro cytotoxicity was assessed using a water-soluble tetrazolium salt-based cell viability assay (EZ-Cytox; Daeil Lab Service, Seoul, Korea) in MCF-7/ADR and L929 fibroblast cells [58]. Briefly, cells were seeded into a 96-well plate at a density of $1.5 \times 10^4$ cells/well and incubated at 37 °C with 5 % $CO_2$ for 1 day. The medium was completely replaced with a suspension of PCN-223-Fe or PCN-223-Fe/L-arg prepared in a culture medium at varying concentrations (0.01, 0.05, 0.1, 0.25, 0.5, 1, 1.5, and 2 mg/ml) and incubated for another 24 h. After that, the medium in each well was replaced with an equal volume of fresh medium, followed by adding 10 μl of an EZ-Cytox reagent, and incubated for 2 h. The plate was assessed by measuring the absorbance at wavelengths of 450 and 600 nm using a microplate reader (SpectraMax 190 Microplate Reader; Molecular Devices, San Jose, CA, USA). Cell viability was calculated using the following equation: Cell viability (%) = (Absorbance at 450 nm of the treated well - Absorbance at 600 nm of the treated well)/(Absorbance at 450 nm of the untreated control well - Absorbance at 600 nm of the untreated control well) × 100.

### 2.8. In vitro anticancer effect evaluation

To assess the anticancer effect of the formulations, MCF-7/ADR cells were seeded in a 96-well plate at a density of $1.5 \times 10^4$ cells/well and incubated for 24 h. Cells were treated with four different formulations: CPT-11 (i.e., an aqueous solution of CPT-11), PCN-223-Fe/CPT-11 (i.e., a suspension of PCN-223-Fe/CPT-11), PCN-223-Fe/L-arg + CPT-11 (i.e., a mixture of PCN-223-Fe/L-arg suspension and CPT-11 solution), or PCN-223-Fe/L-arg + PCN-223-Fe/CPT-11 (a suspension of PCN-223-Fe/L-arg and PCN-223-Fe/CPT-11) at varying equivalent CPT-11 concentrations (3.4, 17, 42.5, 85, 170, and 340 μM CPT-11) and fixed PCN-223-Fe/L-arg concentration (1 mg/ml). After incubation for 48 h, the medium in each well was replaced with an equal volume of fresh medium, followed by the addition of 10 μl of an EZ-Cytox reagent, and incubated for 2 h. Cell viability was calculated by the equation described above.

### 2.9. In vivo evaluation

The protocol for animal experiments was approved by the Institutional Animal Care and Use Committee (IACUC no. 19-0250-C1A0) at Seoul National University Hospital Biomedical Research Institute. For in vivo evaluation, mice bearing MCF-7/ADR cells were prepared. The cell suspension ($2 \times 10^6$ cells) prepared in Matrigel® (Corning, New York, NY, USA) was subcutaneously implanted with 6-week-old BALB/c female nude mice. When the tumor volume reached 100 $mm^3$, mice were randomly selected to be assigned into seven groups (n = 4 per group): (1) no treatment (i.e., no injections), (2) PCN-223-Fe (i.e., intratumoral injections of a PCN-223-Fe suspension), (3) PCN-223-Fe/L-arg (i.e., intratumoral injections of a PCN-223-Fe/L-arg suspension), (4) CPT-11 (i.e., intratumoral injections of a CPT-11 solution), (5) PCN-223-Fe/CPT-11 (i.e., intratumoral injections of a PCN-223-Fe/CPT-11 suspension), (6) PCN-223-Fe/L-arg + CPT-11 (i.e., intratumoral injections of a mixture of a PCN-223-Fe/L-arg suspension and CPT-11 solution), and (7) PCN-223-Fe/L-arg + PCN-223-Fe/CPT-11 (i.e., intratumoral injections of a mixture of a PCN-223-Fe/L-arg and PCN-223-Fe/CPT-11 suspension). For each injection, the CPT-11 and L-arg doses were 5 and 18.75 mg/kg, respectively (i.e., an approximate daily dose of 1.67 and 6.25 mg/kg, respectively [59]), and the amount of administered PCN-223-Fe was 2 mg. For each animal, injection was performed once every 3 days for 21 days.

At scheduled times after treatment, the tumor volume and body weight were measured to assess the antitumor efficacy and safety of the formulations, respectively. To assess the tumor volume, the shortest (d) and longest (D) diameters of the tumor from the skin outside were measured using a Vernier caliper (CD-15APX; Mitutuyo Corporation, Sakado, Japan), with which the tumor volume was calibrated using the following equation: tumor volume = $d^2 \times D/2$ [60]. At the end of the experiments (21 days after treatment), the animal was sacrificed by $CO_2$ asphyxiation, and the tumor was biopsied. Tumor tissue was fixed in 4 % neutral buffered formalin, embedded in paraffin, and sectioned in 4-μm-thick slices to prepare the tissue slides. To examine the anticancer effect, H&E staining and TUNEL assay were carried out. For H&E staining, the slide was dipped with a hematoxylin solution for 10 min and washed with DI water and a mixed solution of HCl and 70 % ethanol. The slide was immersed in an eosin Y solution for 1 min and dehydrated with xylene and ethanol. For the TUNEL assay, a commercial kit (No.

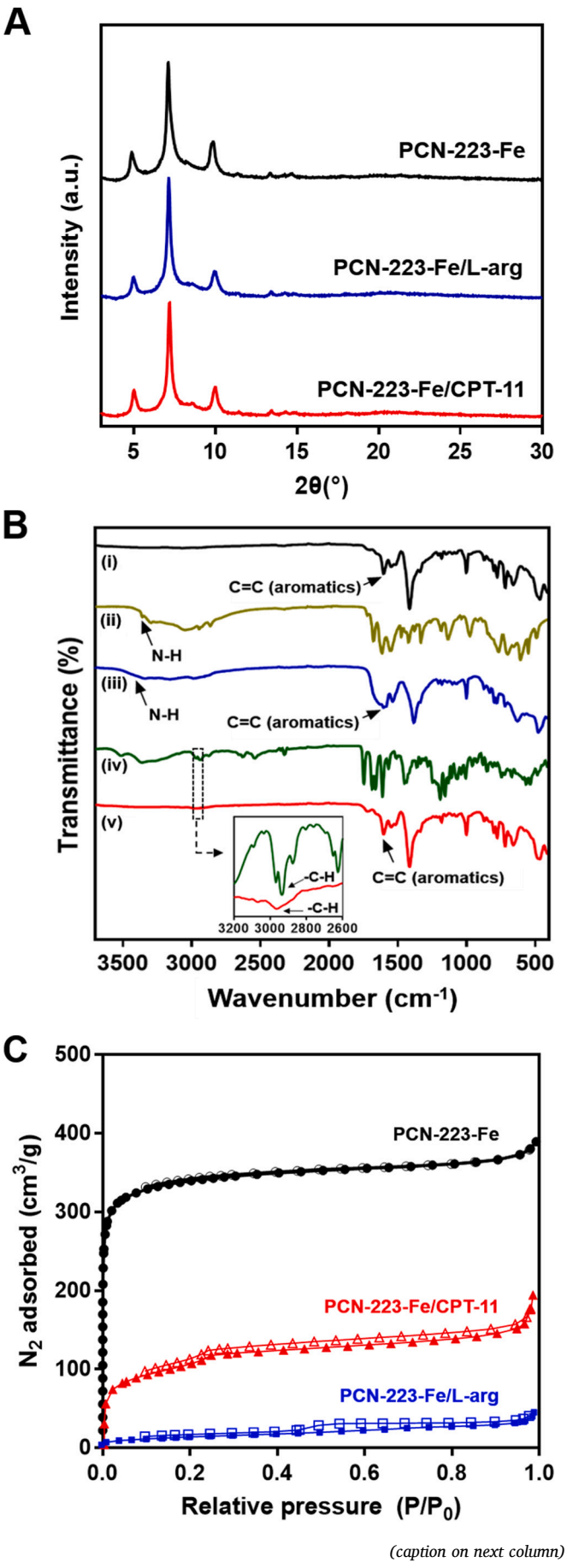


(caption on next column)

**Fig. 1.** Characterization of PCN-223-Fe, PCN-223-Fe/L-arg, and PCN-223-Fe/CPT-11. (A) XRD patterns of PCN-223-Fe, PCN-223-Fe/L-arg, and PCN-223-Fe/CPT-11. (B) FTIR spectra of (i) PCN-223-Fe, (ii) L-arg, (iii) PCN-223-Fe/L-arg, (iv) CPT-11, and (v) PCN-223-Fe/CPT-11. (C) $N_2$ isotherm profiles of PCN-223-Fe, PCN-223-Fe/L-arg, and PCN-223-Fe/CPT-11. ●, PCN-223-Fe adsorption; ○, PCN-223-Fe desorption; ▲, PCN-223-Fe/CPT-11 adsorption; △, PCN-223-Fe/CPT-11 desorption; ■, PCN-223-Fe/L-arg adsorption; □, PCN-223-Fe/L-arg desorption.

11684817910; Roche, Basel, Switzerland) was used to stain the slides according to the manufacturer's protocol. The image of the stained slide was obtained at ×40 magnification using an optical microscope (ECLIPSE Ts2; Nikon, Tokyo, Japan). P-gp expression in tumor tissue was examined by immunofluorescence staining. Briefly, the tissue slide was incubated with an anti-P-gp antibody (1:500; ab129450; Abcam, Cambridge, MA, USA) overnight at 4 °C. After washing with PBS, the slide was incubated with a secondary antibody (1:500; Alexa Flour® 488; ab150077; Abcam) for 1 h at room temperature. The stained cells were counterstained by 4′6-diamidino-2-phenylindole (Sigma, St. Louis, MO, USA) to visualize the nuclei. The image of the stained slide was obtained at ×200 magnification using a CLSM (TCS SP8 STED CW; Leica Microsystems). For each analysis, five tissue slides were assessed from each animal. Thus, 20 tissue slides were examined for each animal group. All tissue images were assessed by a professional pathologist (C. L.).

### 2.10. Statistical analysis

Data were reported as the mean ± standard deviation. The cell viability and tumor volume values were statistically analyzed using the Mann-Whitney *U* test (GraphPad Prism 7.0; GraphPad Software, San Diego, CA, USA). In all cases, a 95 % confidence level ($p < 0.05$) was considered to represent a statistical difference in the data (*$p < 0.05$; **$p < 0.01$).

## 3. Results

### 3.1. Characterization of PCN-223-Fe and its formulation

In this study, PCN-223-Fe was synthesized by the solvothermal method [51], in which L-arg or CPT-11 was loaded via physical adsorption into the pores. The X-ray diffraction (XRD) patterns clearly exhibited the structural feature and crystallinity of PCN-223-Fe [42], which was maintained with PCN-223-Fe/L-arg and PCN-223-Fe/CPT-11 after L-arg and CPT-11 loading, respectively (Fig. 1A). This study also examined Fourier transform infrared (FTIR) spectra (Fig. 1B), where PCN-223-Fe exhibited the characteristic peaks at 1601 $cm^{-1}$ owing to the C—C stretching in the aromatic ring [61]. The typical stretching frequency of L-arg included N—H stretching at 3357 $cm^{-1}$ [62]. CPT-11 exhibited the characteristic peaks at 2968 $cm^{-1}$, attributed to $sp^3$ C—H stretching in the methyl group [63]. For PCN-223-Fe/L-arg and PCN-223-Fe/CPT-11, the characteristic bands from PCN-223-Fe and the loaded compound overlapped without any apparent shift, implying that their chemical structures were not altered after encapsulation. Fig. 1C shows the $N_2$ adsorption-desorption isotherms of PCN-223-Fe, PCN-223-Fe/L-arg, and PCN-223-Fe/CPT-11. All exhibited type I pattern isotherms, confirming that their microporous structure was maintained before and after compound loading. However, in Table 1, the surface area and pore volume decreased in PCN-223-Fe/L-arg and PCN-223-Fe/CPT-11, indicating the presence of encapsulated molecules in the pores of PCN-223-Fe. For PCN-223-Fe/L-arg and PCN-223-Fe/CPT-11, the loading amount of L-arg and CPT-11 was measured as 250 ± 7 and 210 ± 4 μg/mg, respectively (Table 1).

Scanning electron microscopy (SEM) and transmission electron microscopy (TEM) images exhibited that PCN-223-Fe was fabricated as spindle-shaped particles, 1 to 2 μm long, as reported previously (Fig. 2A,

**Table 1**
Brunauer-Emmett-Teller surface areas, pore volumes, and compound loading amounts of PCN-223-Fe, PCN-223-Fe/L-arg, and PCN-223-Fe/CPT-11.

| | PCN-223-Fe | PCN-223-Fe/L-arg | PCN-223-Fe/CPT-11 |
|---|---|---|---|
| Surface area ($m^2$/g) | 1302 | 52 | 372 |
| Pore volume ($cm^3$/g) | 0.6 | 0.07 | 0.29 |
| Loading amount (μg/mg) | – | 250 ± 7 (L-arg) | 210 ± 4 (CPT-11) |

B) [42,51]. This overall shape did not change with PCN-223-Fe/L-arg and PCN-223-Fe/CPT-11 after compound loading. This study also analyzed the size and surface charge of the particles suspended in phosphate-buffered saline (PBS; pH 7.4) by dynamic light scattering (Fig. 2C,D). The average particle size of PCN-223-Fe, PCN-223-Fe/L-arg, and PCN-223-Fe/CPT-11 was not very different, measured to be 806, 763, and 834 nm, respectively. The surface charge of PCN-223-Fe was 33.7 mV, which, however, decreased to 18.8 and 7.7 mV with PCN-223-Fe/L-arg and PCN-223-Fe/CPT-11. In PCN-223-Fe/L-arg, a guanidine moiety of L-arg was adsorbed to an open metal site of PCN-223-Fe, which made a carboxyl acid moiety of L-arg directed to the outer surface of PCN-223-Fe, thereby a decreased surface charge [64,65] (Fig. S1). For PCN-223-Fe/CPT-11, the shift of surface charge was ascribed to the loading of negatively charged CPT-11, respectively [66].

### 3.2. *In vitro profiles of compound release and NO generation*

This study assessed the in vitro release profiles of L-arg and CPT-11. PCN-223-Fe/L-arg and PCN-223-Fe/CPT-11 were each suspended in PBS (pH 5.5), mimicking an acidic environment of the tumor tissue [67,68]. In Fig. 3A, PCN-223-Fe/L-arg and PCN-223-Fe/CPT-11 exhibited a sustained release of L-arg and CPT-11 for up to 3 days, respectively, mainly by out-diffusion of the compound encapsulated within the pores of PCN-223-Fe [69,70]. There was an initial burst release during the first 8 h, which could be due to the presence of the compound distributed on the PCN-223-Fe surface. Therefore, this burst release was slightly lower with CPT-11 due to its lower water solubility than L-arg [71,72]. The L-arg release was less sustained in a simulated environment of the normal tissues due to a relatively faster degradation of PCN-223-Fe at neutral pH, which, however, did not appear to much influence the release

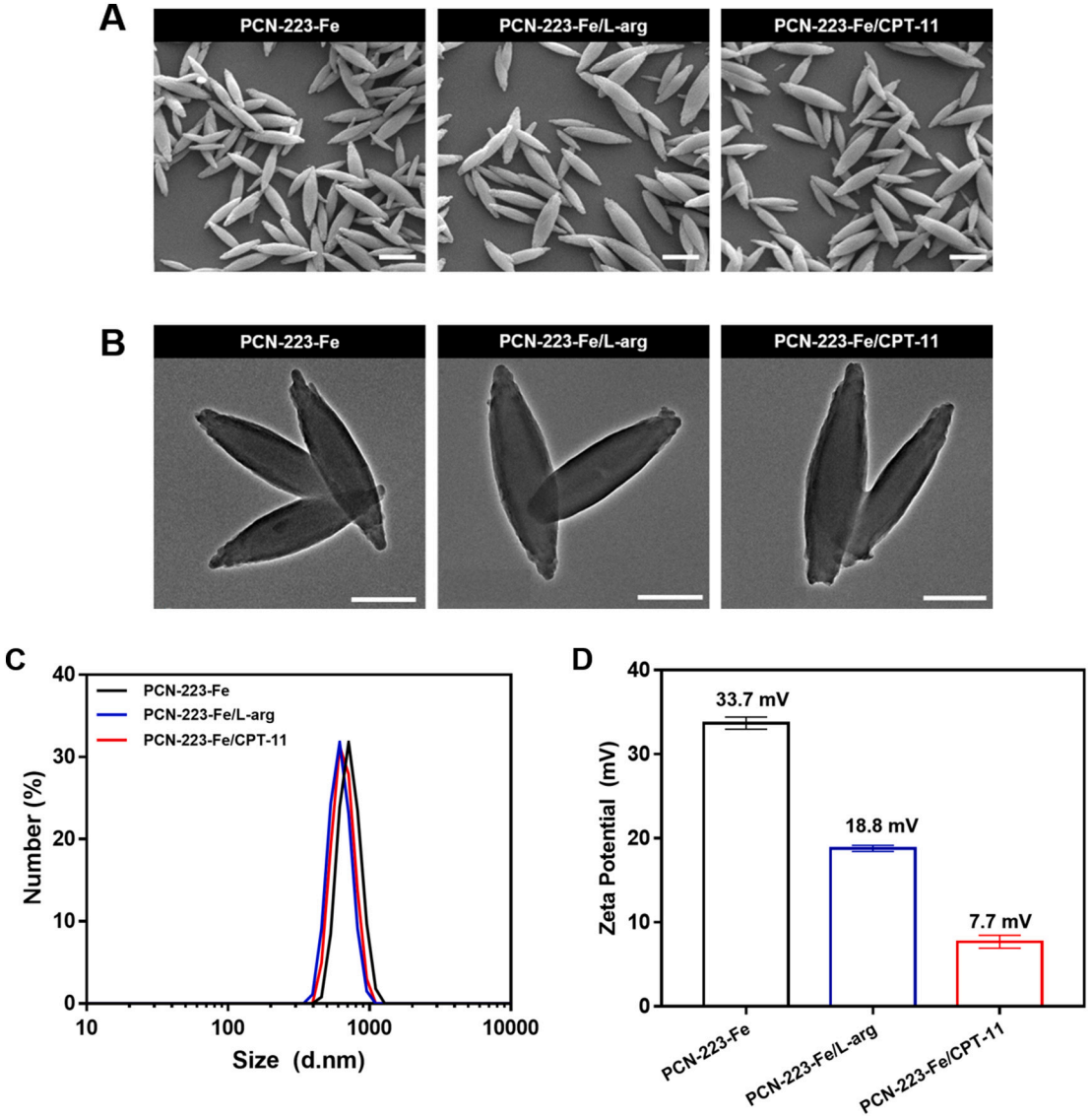


**Fig. 2.** Morphology, size distributions, and zeta potentials of PCN-223-Fe, PCN-223-Fe/L-arg, and PCN-223-Fe/CPT-11. (A) SEM images of PCN-223-Fe, PCN-223-Fe/L-arg, and PCN-223-Fe/CPT-11. Scale bar, 1 μm. (B) TEM images of PCN-223-Fe, PCN-223-Fe/L-arg, and PCN-223-Fe/CPT-11. Scale bar, 500 nm. (C) Size distributions and (D) zeta potentials of PCN-223-Fe, PCN-223-Fe/L-arg, and PCN-223-Fe/CPT-11.

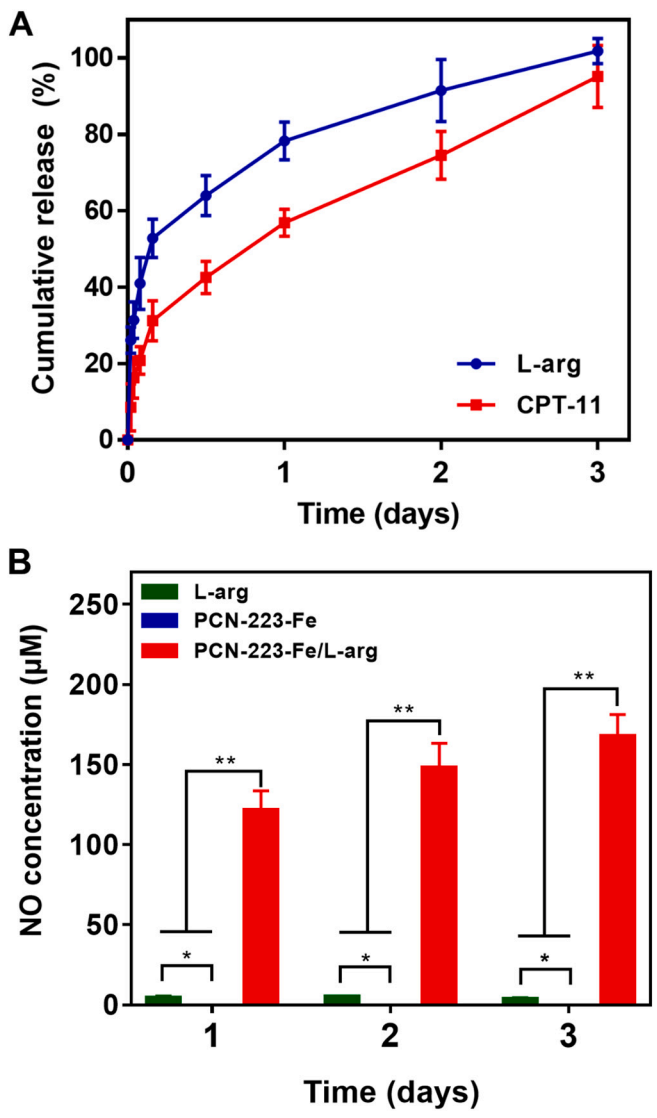


**Fig. 3.** In vitro profiles of compound release and NO generation. (A) In vitro release profiles of L-arg and CPT-11 from PCN-223-Fe/L-arg and PCN-223-Fe/CPT-11, respectively. Error bars represent the SD (n = 3). (B) Concentration profiles of NO while L-arg, PCN-223-Fe, and PCN-223-Fe/L-arg were each added and incubated for 3 days in 6 ml PBS (pH 5.5) containing 100 μM $H_2O_2$. In all conditions, the same amount of L-arg (1.25 mg) or PCN-223-Fe (3.75 mg) was used. Error bars represent the SD (n = 3). *$p < 0.05$, **$p < 0.01$.

profile of less hydrophilic CPT-11 (Fig. S2).

With PCN-223-Fe/L-arg, this study generated NO by the oxidation of L-arg, which would be mediated by endogenous $H_2O_2$ in tumor tissue and catalytic Fe-porphyrin, the organic ligand of PCN-223-Fe. Due to these biomimetic conditions, this study also proposed that a relatively high level of $H_2O_2$ already present in tumor tissue should be sufficient to generate an effective amount of NO for MDR treatment. Thus, this study first assessed the capability of NO generation under simulated tumor environments, where PCN-223-Fe/L-arg was suspended in PBS (pH 5.5) containing 100 μM $H_2O_2$ [73,74]. In Fig. 3B, PCN-223-Fe/L-arg indeed generated NO, the level of which could be considered high enough to reverse the MDR effect [16,75]. The cumulative amount of NO gradually increased for 3 days as observed with sustained release of L-arg (Fig. 3A). Furthermore, when tested under various $H_2O_2$ concentrations, the efficacy in NO generation was clearly observable with PCN-223-Fe/L-arg (Fig. S3). In contrast, only with L-arg, NO was generated to some extent due to the presence of endogenous $H_2O_2$, but the amount was very low (<5 μM). With the PCN-223-Fe only, there was no generation of NO because of the absence of NO donor, L-arg. Those results indicated the necessity of the coexistence of L-arg and PCN-223-Fe.

### 3.3. In vitro cell tests

PCN-223-Fe as carriers of L-arg or CPT-11 could be delivered into MDR cells to release the encapsulated compound. Thus, this study first analyzed the intracellular uptake profile of PCN-223-Fe using MDR cancer cells (i.e., MCF-7/ADR cells). For this, PCN-223-Fe was loaded with a fluorescence probe instead, calcein (~360 μg/mg), with which cells were treated and assessed by flow cytometry [56,57]. In Fig. 4A, PCN-223-Fe was efficiently delivered into cells within 2 h at all concentrations tested in this study. During this period of cell exposure, >90 % calcein was still entrapped in the PCN-223-Fe (Fig. S4), and it is known that free calcein molecules cannot be taken inside the cells [76].

Given those, this study assessed the degree of NO generation with PCN-223-Fe/L-arg. Cells were incubated with different L-arg-based formulations and treated with 3-amino,4-aminomethyl-2′,7′-difluorescein diacetate (DAF-DA), a dye that reacts with NO to emit green fluorescence [20]. According the results from the confocal fluorescence microscopic images in Fig. 4B, cells treated with PCN-223-Fe/L-arg showed the strongest fluorescence signal among the tested formulations, suggesting a significant amount of NO generated in cells. A weak signal from cells treated solely with L-arg or PCN-223-Fe was not different from that of cells without treatment, which could be ascribed to endogenous NO already present inside the cells [77]. In Fig. 4C, PCN-223-Fe and PCN-223-Fe/L-arg exhibited negligible cytotoxicity at all concentrations tested in this study. This result indicated that PCN-223-Fe and loaded L-arg and the generated NO had no adverse effects on cell viability. This noncytotoxic response was also observed when PCN-223-Fe and PCN-223-Fe/L-arg were tested in L929 mouse fibroblast cells (Fig. S5).

For treatment of MDR cancer, this study proposed a codelivery of PCN-223-Fe/L-arg and PCN-223-Fe/CPT-11. Therefore, to examine the efficacy, MCF-7/ADR cells were treated with four different formulations at varying doses of CPT-11, as shown in Fig. 4D. For all formulations, an anticancer effect of CPT-11 was observable: cell viability gradually decreased as CPT-11 concentration increased. However, the anticancer effect was most prominent when PCN-223-Fe/L-arg and PCN-223-Fe/CPT-11 were delivered together, where cell viability was significantly lower than the other three different formulations from and above the CPT-11 concentration of 45 μM ($p < 0.05$). Thus, PCN-223-Fe as carriers would be engulfed into cells efficiently, where NO and CPT-11 would be exposed in a sustained manner, thereby much improved anticancer effects on MDR cancer cells.

### 3.4. In vivo evaluations

For in vivo evaluation, mice bearing MCF-7/ADR cancer cells were treated with intratumoral injections of seven formulations: (1) no treatment (i.e., no injections), (2) PCN-223-Fe, (3) PCN-223-Fe/L-arg, (4) CPT-11, (5) PCN-223-Fe/CPT-11, (6) PCN-223-Fe/L-arg + CPT-11, and (7) PCN-223-Fe/L-arg + PCN-223-Fe/CPT-11. In Fig. 5A, groups without CPT-11 treatment (i.e., no treatment, PCN-223-Fe, and PCN-223-Fe/L-arg groups) exhibited an evident tumor growth profile. Moderate inhibition of tumor growth was observed when a bolus CPT-11 was injected (i.e., with the CPT-11 group), which was significantly lower than that of the groups without CPT-11 treatment at 21 days ($p < 0.05$). However, this was not very different from that of the PCN-223-Fe/CPT-11 group, implying that more efficient intracellular delivery and sustained exposure of CPT-11 alone would not be able to effectively treat MDR cancer. The effect of NO generation from PCN-223-Fe/L-arg was clearly observable when injected together with CPT-11. A bolus injection of CPT-11, when combined with PCN-223-Fe/L-arg treatment, exhibited a significantly smaller tumor volume from 18 days than the CPT-11 group.

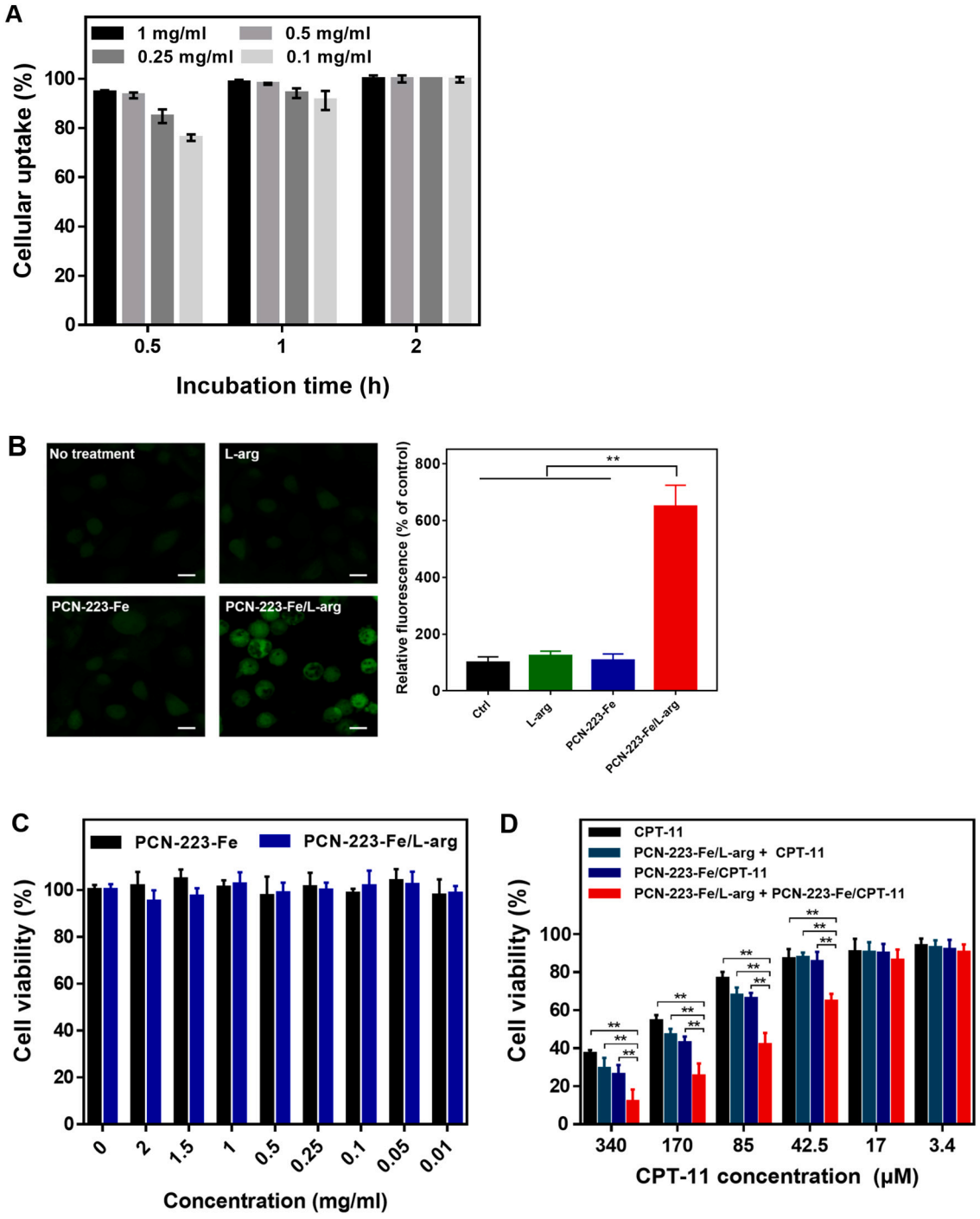


**Fig. 4.** In vitro cell tests. (A) Profiles of intracellular uptake of calcein-loaded PCN-223-Fe measured by flow cytometry. Error bars represent the SD (n = 3). (B) Representative confocal fluorescence images and quantitative data of fluorescence intensity obtained from cells without treatment and those treated with L-arg, PCN-223-Fe, and PCN-223-Fe/L-arg. Cells were probed by DAF-DA to assess the presence of NO. In all conditions, the same concentration of L-arg (125 μg/ml) or PCN-223-Fe (500 μg/ml) was used. Scale bar, 10 μm. Error bars represent the SD (n = 4). **$p < 0.01$. (C) Cytotoxicity test results with PCN-223-Fe and PCN-223-Fe/L-arg. The varying concentrations were based on the equivalent amount of PCN-223-Fe. Error bars represent the SD (n = 6). (D) Cell viability evaluation after treatment with four different formulations: (1) CPT-11, (2) PCN-223-Fe/L-arg + CPT-11, (3) PCN-223-Fe/CPT-11, and (4) PCN-223-Fe/L-arg + PCN-223-Fe/CPT-11. In all conditions, the PCN-223-Fe/L-arg concentration was 1 mg/ml. The varying concentrations were based on the equivalent amount of CPT-11. Error bars represent the SD (n = 6). **$p < 0.01$.

Notably, the most prominent tumor suppression effect was observed when PCN-223-Fe/L-arg and PCN-223-Fe/CPT-11 were injected together. For a whole period of 21 days, tumor growth was seen to be minimal (<23 %); thus, this was significantly lower than that of all other groups from 9 days ($p < 0.05$). As proposed with the current strategy, after intratumoral injection, PCN-223-Fe/L-arg and PCN-223-Fe/CPT-11 would be efficiently delivered into cells; after which those would generate NO and release CPT-11 in a sustained manner, respectively. This result indicated that the amount of generated NO was sufficient to reverse MDR, which could improve the availability of CPT-11 in cells to effectively suppress tumor growth under in vivo environmental conditions. More importantly, this synergistic effect could be obtained with

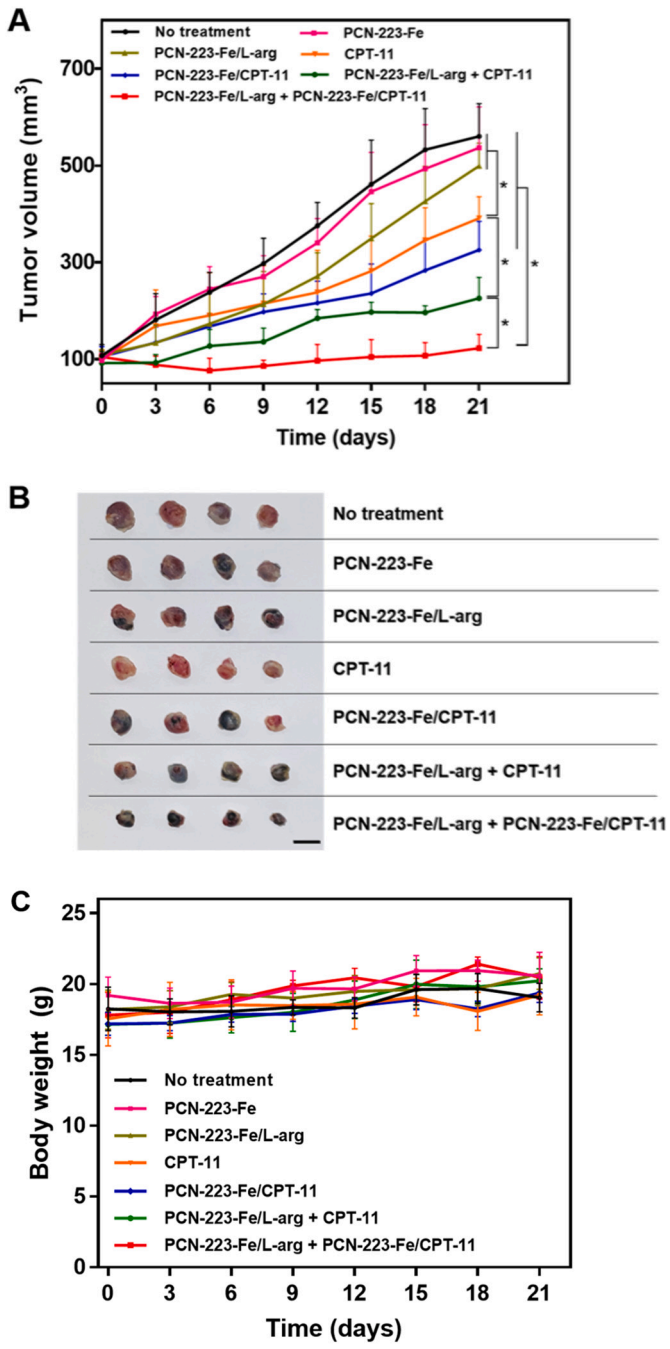


**Fig. 5.** In vivo evaluation results. In vivo evaluation test was performed using seven animal groups: (1) no treatment, (2) PCN-223-Fe, (3) PCN-223-Fe/L-arg, (4) CPT-11, (5) PCN-223-Fe/CPT-11, (6) PCN-223-Fe/L-arg + CPT-11, and (7) PCN-223-Fe/L-arg + PCN-223-Fe/CPT-11. For each animal, the formulation was injected intratumorally once every 3 days for 21 days. For the relevant groups, the CPT-11 and L-arg doses were 5 and 18.75 mg/kg, respectively. (A) Tumor growth profiles. Error bars represent the SD (n = 4). *p < 0.05. (B) Representative optical images of whole tumor tissues biopsied at the endpoint of the experiments (21 days). Scale bar, 1 cm. (C) Body weight profiles. Error bars represent the SD (n = 4).

biomimetic compounds in the formulation, i.e., the catalyst present in PCN-223-Fe and NO donor, L-arg, thereby no additional process for ROS generation generally employed to produce NO. In Fig. 5B, the PCN-223-Fe/L-arg and PCN-223-Fe/CPT-11 groups exhibited the smallest volume of tumor tissue biopsied at the endpoint of the experiments. During the whole testing period, there was almost no change in body weight in all groups, implying no apparent toxicity of PCN-223-Fe-based formulations (Fig. 5C).

To further confirm the efficacy of the suggested formulation, histopathologic analysis was first performed on tumor tissue biopsied at the endpoint of the experiments. In Fig. 6A, tissue on hematoxylin and eosin (H&E) staining exhibited a large area of cell shrinkage and nuclear fragmentation in the PCN-223-Fe/L-arg + PCN-223-Fe/CPT-11 group. Based on the images of tumor tissue on terminal deoxynucleotidyl transferase-mediated dUTP nick end labeling (TUNEL; Fig. 6B), enhanced apoptosis and cell death were also clearly observed in the PCN-223-Fe/L-arg + PCN-223-Fe/CPT-11 group. This study also sought to find P-gp expression in tumor tissue, representing the expression of efflux pumps located in the membrane of MDR cells [78,79]. For this, immunofluorescence analysis was performed on the tissue (Fig. 6C), where all groups treated with PCN-223-Fe/L-arg showed weaker green fluorescence, indicating suppressed P-gp expression by NO generation.

## 4. Discussion

Due to its important physiological and biological roles, various studies have been conducted to effectively deliver NO in the body [80]. In this aspect, MOF has drawn a great deal of interest as the high porosity and large specific surface area allow MOF as carriers of gaseous NO itself or NO donors [81–83]. However, gaseous NO adsorbed in MOF is not easily desorbed, thereby reducing NO delivery efficiency [81]. NO could be generated by catalytic reactions with the NO donor loaded in MOF; however, metal ions in MOF essential for this reaction, such as Cu or Co, were not biocompatible [26,71]. A composite of a biocompatible polymer and MOF was introduced to lower the amount of these metals in the formulation, but this also reduced the amount of MOF together, hence low efficiency of NO generation again [84–86]. Synthetic NO donors are not yet optimized: *S*-nitrosocysteine was not stable even after encapsulation, and *S*-nitrosothiol produced a toxic byproduct after NO generation [29]. Therefore, a biological NO donor, arginine, was employed and loaded in MOF composed of biocompatible metals, such as Zr or Fe [35,36]. With those formulations, a therapeutically effective amount of NO could be generated by an additional excessive delivery of ROS, which may damage the surrounding normal tissue [36–39,87].

In living organisms, a biosynthetic pathway for NO is based on the oxidation reaction of L-arg catalyzed by NOS without toxic byproducts or participation of additional ROS. A heme structure in NOS contains a Fe ion coordinated to a porphyrin, which plays a key role in the oxidative transformation of endogenous and exogenous molecules [88]. However, free molecules of Fe-containing porphyrin are inherently not stable as they would self-aggregate by π-π stacking between porphyrin rings, hence the loss of its catalytic activity [45]. Given those, PCN-223-Fe/L-arg would be advantageous as a formulation for biomimetic NO generation. PCN-223-Fe is composed of a metallic center of a biocompatible Zr bridged with the ligands of Fe-porphyrin, and this specific structure allows Fe-porphyrin to be immobilized and independent, hence retaining its catalytic activity [42]. This integrity could be better retained under physiological conditions of cancerous environments (Fig. S6).

Results revealed that, through the porous structure of PCN-223-Fe, L-arg was released in a sustained manner for 3 days, during which NO was also generated continuously through a catalytic reaction between biomimetic compounds, i.e., the released L-arg and ligand of Fe-porphyrin in PCN-223-Fe (Fig. 3). Thus, this NO generation profile could be obtained under an endogenous condition of $H_2O_2$ without its additional production or delivery, where the $H_2O_2$ concentration was set at a level found in MDR cells [47]. PCN-223-Fe in a spindle shape was observed to be internalized efficiently to cells (Fig. 4A), which could be ascribed to the proper size and sharp edges of the particles, as well as a positive surface charge of the PCN-223-Fe (Fig. 2) [69,89,90]. Those particles produced NO inside MDR cells at a profound level (Fig. 4B). With this high efficiency in intracellular uptake, PCN-223-Fe and the NO-

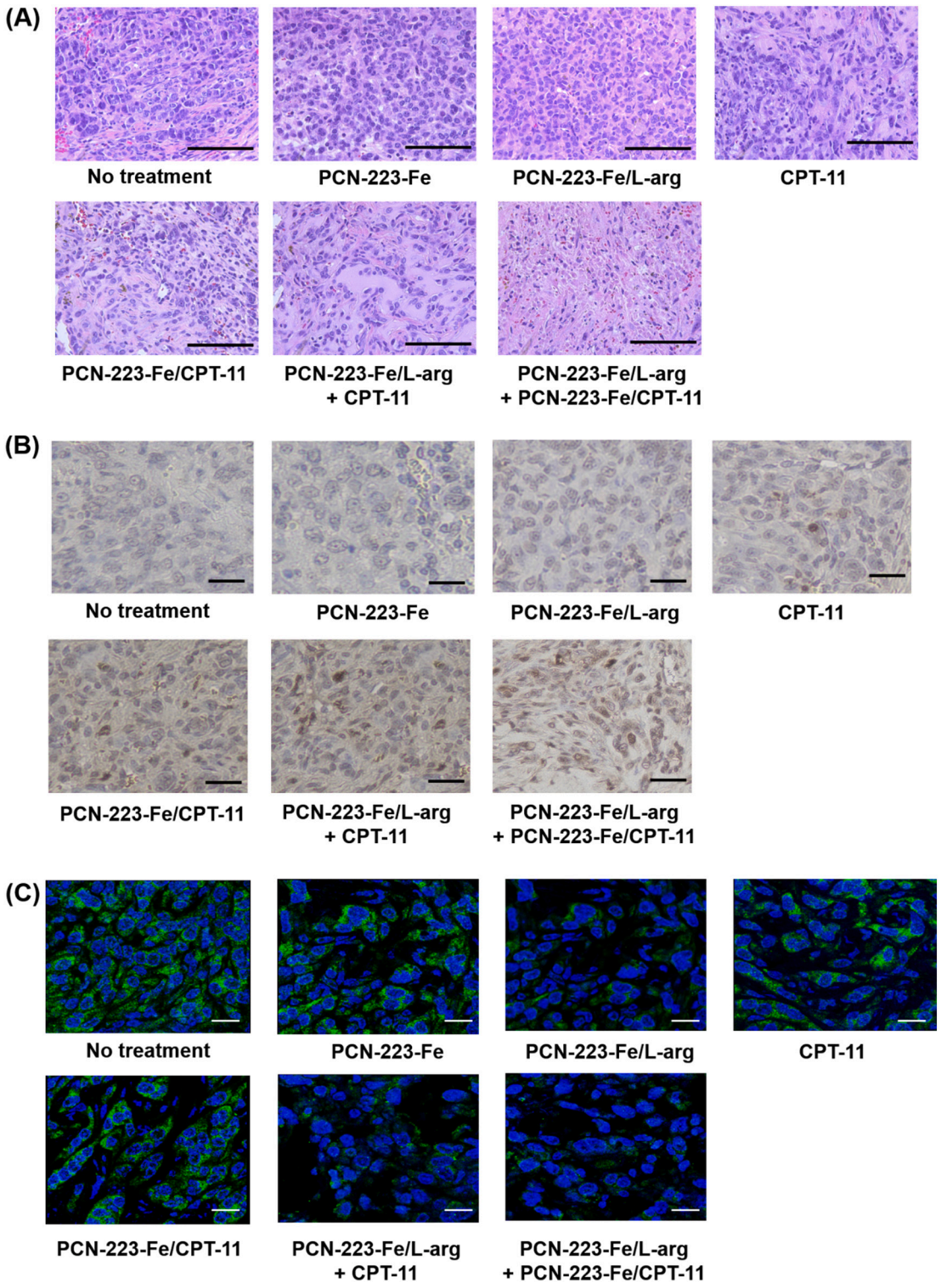


**Fig. 6.** Histopathologic analysis. (A) H&E-stained tissue images. Scale bar, 50 μm. (B) TUNEL-stained tissue images. Scale bar, 10 μm. (C) Immunofluorescence images of tumor tissue stained in green for P-pg expression. Scale bar, 10 μm. (For interpretation of the references to colour in this figure legend, the reader is referred to the web version of this article.)

generating PCN-223-Fe/L-arg exhibited almost no cytotoxicity after internalization to cells due to the biocompatibility of all composing materials, i.e., Zr, Fe-porphyrin and L-arg (Fig. 4C and Fig. S5) [31,40,91]. In this work, the PCN-223-Fe based formulations were used freshly after synthesis for each experiment. However, a long-term stability of those nanoparticles may need to be considered in an aspect of a shelf-life.

In this study, PCN-223-Fe was also employed as carriers of an anticancer drug, CPT-11. Thus, the combined formulation of PCN-223-Fe/L-arg and PCN-223-Fe/CPT-11 was suggested to treat MDR tumors. For codelivery with PCN-223-Fe/L-arg, PCN-223-Fe/CPT-11 was designed to release the drug in a sustained manner for the same period of 3 days (Fig. 3A). Compared to other control groups, the combined formulation exhibited a prominent anticancer effect on MDR cells (Fig. 4D). The in

vivo results also revealed that implanted MDR tumors did not grow much when treated with the combined formulation (Fig. 5A, B), significantly lower than animals treated with the same dose of CPT-11. This result further confirmed that the level of NO generation with PCN-223-Fe/L-arg was sufficient to reverse the MDR effect and increase the intracellular availability of CPT-11, which was synergistically improved when CPT-11 was released in a sustained manner from PCN-223-Fe/CPT-11. P-gp expression was indeed downregulated with cells in the biopsied tissue of animals treated with PCN-223-Fe/L-arg (Fig. 6C). Notably, this therapeutic condition was obtained with the endogenous $H_2O_2$ already present in MDR tumor cells under in vivo environments, which was possible with biomimetic compounds of L-arg and Fe-porphyrin in PCN-223-Fe and the endogenous mechanism of NO production (Scheme 1). After completed compound release, the cancerous cells would be apoptosed and lysed to release the carrier, PCN-223-Fe, which would be diffused to the surrounding normal tissues to be eventually degraded and cleared at pH 7.4 (Fig. S6). The degradation byproducts of PCN-223-Fe, such as Zr and Fe-porphyrin, were reported to be biocompatible [40,91]. Those led to the safety of the formulation as the health of the animals did not appear to be affected even after multiple repeated doses (Fig. 5C).

## 5. Conclusion

PCN-223-Fe was proposed as a carrier material for anticancer drug therapy on MDR cancer. PCN-223-Fe, a type of MOF, possesses a highly porous structure into which L-arg or CPT-11 can be encapsulated and released in a sustained manner. Importantly, a ligand of Fe-porphyrin in PCN-223-Fe can serve as a catalyst to generate NO in a biomimetic pathway. Thus, PCN-223-Fe/L-arg can generate sufficient NO in endogenous cancer environments to reverse MDR without any addition of ROS. For treatment of MDR cancer, this study suggested the codelivery of PCN-223-Fe/L-arg and PCN-223-Fe/CPT-11. This combined formulation can significantly suppress tumor growth in an MDR cancer animal model due to a synergistic effect of NO generation to inhibit P-gp expression and CPT-11, an anticancer drug. Therefore, PCN-223-Fe-based formulation can be a promising strategy for treating MDR cancer.

## Data availability

Data will be made available on request.

### *Acknowledgments*

This research was supported by the Basic Science Research Program through the National Research Foundation of Korea (NRF), funded by the Ministry of Science, ICT & Future Planning (NRF-2021R1A2B5B03001914). This work was also financially supported by the Ministry of Trade, Industry and Energy (MOTIE) and Korea Institute for Advancement of Technology (KIAT) through the International Cooperative R&D program. (Project No. P0017190).

### *CRediT authorship contribution statement*

Han Bi Ji: Conceptualization, Methodology, Validation, Formal analysis, Investigation, Resources, Data Curation, Writing – Original Draft, Visualization.

Se-Na Kim: Conceptualization, Methodology, Validation, Formal analysis, Investigation, Resources, Data Curation, Writing – Original Draft, Visualization.

Cho Rim Kim: Validation.

Chang Hee Min: Methology.

Jae Hoon Han: Methology.

Min JI Kim: Methology.

Cheol Lee: Formal analysis.

Young Bin Choy: Conceptualization, Methodology, Validation, Writing – Original Draft, Writing – Review & Editing, Project administration, Funding acquisition.

### *Declaration of competing interest*

The authors declare the following financial interests/personal relationships which may be considered as potential competing interests:

Young Bin Choy reports financial support was provided by National Research Foundation of Korea, and Ministry of Trade, Industry and Energy and Korea Institute for Advancement of Technology. Young Bin Choy, Han Bi Ji and Se—Na Kim has patent #PCT/KR2022/013316 pending to Seoul National University R&DB Foundation.

## Appendix A. Supplementary data

Supplementary data to this article can be found online at https://doi.org/10.1016/j.bioadv.2022.213268.

## References

[1] J.A. Moscow, T. Fojo, R.L. Schilsky, The evidence framework for precision cancer medicine, Nat. Rev. Clin. Oncol. 15 (2018) 183–192, https://doi.org/10.1038/nrclinonc.2017.186.
[2] M.M. Gottesman, T. Fojo, S.E. Bates, Multidrug resistance in cancer: role of ATP–dependent transporters, Nat. Rev. Cancer 2 (2002) 48–58, https://doi.org/10.1038/nrc706.
[3] K. Bukowski, M. Kciuk, R. Kontek, Mechanisms of multidrug resistance in cancer chemotherapy, Int. J. Mol. Sci. 21 (2020) 3233, https://doi.org/10.3390/ijms21093233.
[4] J.P. Gillet, M.M. Gottesman, in: Mechanisms of Multidrug Resistance in Cancer, Humana Press, 2010, pp. 47–76, https://doi.org/10.1007/978-1-60761-416-6_4.
[5] S. Kunjachan, B. Rychlik, G. Strom, F. Kiessling, T. Lammers, Multidrug resistance: physiological principles and nanomedical solutions, Adv. Drug Deliv. Rev. 65 (2013) 1852–1865, https://doi.org/10.1016/j.addr.2013.09.018.
[6] A.A. Stavrovskaya, Cellular mechanisms of multidrug resistance of tumor cells, Biochem. Biokhim. 65 (2000) 95–106.
[7] Y.H. Choi, A.M. Yu, ABC transporters in multidrug resistance and pharmacokinetics, and strategies for drug development, Curr. Pharm. Des. 20 (2014) 793–807.
[8] J.A. Shabbits, R. Krishna, L.D. Mayer, Molecular and pharmacological strategies to overcome multidrug resistance, Expert. Rev. Anticancer. Ther. 1 (2001) 585–594, https://doi.org/10.1586/14737140.1.4.585.
[9] R. Callaghan, F. Luk, M. Bebawy, Inhibition of the multidrug resistance P-glycoprotein: time for a change of strategy? Drug Metab. Dispos. 42 (2014) 623–631, https://doi.org/10.1124/dmd.113.056176.
[10] A. Persidis, Cancer multidrug resistance, Nat. Biotechnol. 17 (1999) 94–95, https://doi.org/10.1038/5289.
[11] Y.G. Assaraf, A. Brozovic, A.C. Goncalves, D. Jurkovicova, A. Line, M. Machuqueiro, S. Saponara, A.B. Sarmento-Ribeiro, C.P.R. Xavier, M. H. Vasconcelos, The multi-factorial nature of clinical multidrug resistance in cancer, Drug Resist. Updat. 46 (2019), 100645, https://doi.org/10.1016/j.drup.2019.100645.
[12] M. Magierowski, K. Magierowska, S. Kwiecien, T. Brzozowski, Gaseous mediators nitric oxide and hydrogen sulfide in the mechanism of gastrointestinal integrity, protection and ulcer healing, Molecules 20 (2015) 9099–9123, https://doi.org/10.3390/molecules20059099.
[13] M.L.L. Faro, B. Fox, J.L. Whatmore, P.G. Winyard, M. Whiteman, Hydrogen sulfide and nitric oxide interactions in inflammation, Nitric Oxide 41 (2014) 38–47, https://doi.org/10.1016/j.niox.2014.05.014.
[14] L.G. Branco, Gaseous mediators in temperature regulation, Compr. Physiol. 4 (2014) 1301–1338, https://doi.org/10.1002/cphy.c130053.
[15] J. Kim, B.C. Yung, W.J. Kim, X. Chen, Combination of nitric oxide and drug delivery systems: tools for overcoming drug resistance in chemotherapy, J. Control. Release 263 (2017) 223–230, https://doi.org/10.1016/j.jconrel.2016.12.026.
[16] G. Wei, G. Yang, B. Wei, Y. Wang, S. Zhou, Near-infrared light switching nitric oxide nanoemitter for triple-combination therapy of multidrug resistant cancer, Acta Biomater. 100 (2019) 365–377, https://doi.org/10.1016/j.actbio.2019.10.002.
[17] R. Sullivan, C.H. Graham, Chemosensitization of cancer by nitric oxide, Curr. Pharm. Des. 14 (2008) 1113–1123, https://doi.org/10.2174/138161208784246225.
[18] L.B. Vong, Y. Nagasaki, Nitric oxide nano-delivery systems for cancer therapeutics: advances and challenges, Antioxidants 9 (2020) 791, https://doi.org/10.3390/antiox9090791.
[19] L. Gao, B. Dong, J. Zhang, Y. Chen, H. Qiao, Z. Liu, E. Chen, Y. Dong, C. Cao, D. Huang, W. Chen, Functional biodegradable nitric oxide donor-containing polycarbonate-based micelles for reduction-triggered drug release and overcoming multidrug resistance, ACS Macro Lett. 8 (2019) 1552–1558, https://doi.org/10.1021/acsmacrolett.9b00758.

[20] S. Li, X. Song, W. Zhu, Y. Chen, R. Zhu, L. Wang, X. Chen, J. Song, H. Yang, Light-switchable yolk–mesoporous shell UCNPs@ MgSiO3 for nitric oxide-evoked multidrug resistance reversal in cancer therapy, ACS Appl. Mater. Interfaces 12 (2020) 30066–30076, https://doi.org/10.1021/acsami.0c06102.
[21] L.J. Ignarro, C. Napoli, J. Loscalzo, Nitric oxide donors and cardiovascular agents modulating the bioactivity of nitric oxide: an overview, Circ. Res. 90 (2002) 21–28, https://doi.org/10.1161/hh0102.102330.
[22] Q. He, Precision gas therapy using intelligent nanomedicine, Biomater. Sci. 5 (2017) 2226–2230, https://doi.org/10.1039/C7BM00699C.
[23] P.G. Wang, M. Xian, X. Tang, X. Wu, Z. Wen, T. Cai, A.J. Janczuk, Nitric oxide donors: chemical activities and biological applications, Chem. Rev. 102 (2002) 1091–1134, https://doi.org/10.1021/cr000040l.
[24] S. Huerta, S. Chilka, B. Bonavida, Nitric oxide donors: novel cancer therapeutics, Int. J. Oncol. 33 (2008) 909–927, https://doi.org/10.3892/ijo_00000079.
[25] J. Zhang, H. Song, S. Ji, X. Wang, P. Huang, C. Zhang, W. Wang, D. Kong, NO prodrug-conjugated, self-assembled, pH-responsive and galactose receptor targeted nanoparticles for co-delivery of nitric oxide and doxorubicin, Nanoscale 10 (2018) 4179–4188, https://doi.org/10.1039/C7NR08176F.
[26] Y. Zhou, T. Yang, R. Namivandi-Zangeneh, C. Boyer, K. Liang, R. Chandrawati, Copper-doped metal–organic frameworks for the controlled generation of nitric oxide from endogenous S-nitrosothiols, J. Mater. Chem. B 9 (2021) 1059–1068, https://doi.org/10.1039/D0TB02709J.
[27] H.T.T. Duong, Z.M. Kamarudin, R.B. Erlich, Y. Li, M.W. Jones, M. Kavallaris, C. Boyer, T.P. Davis, Intracellular nitric oxide delivery from stable NO-polymeric nanoparticle carriers, Chem. Commun. 49 (2013) 4190–4192, https://doi.org/10.1039/C2CC37181B.
[28] Y.S. Jo, A.J.V.D. Vilies, J. Gantz, T.N. Thancher, S. Antonijevic, S. Cavadini, D. Demurtas, N. Stergiopulos, J.A. Hubbell, Micelles for delivery of nitric oxide, J. Am. Chem. Soc. 131 (2009) 14413–14418, https://doi.org/10.1021/ja905123t.
[29] K.D. Kröncke, C.V. Suschek, Adulterated effects of nitric oxide–generating donors, J. Invest. Dermatol. 128 (2008) 258–260, https://doi.org/10.1038/sj.jid.5701162.
[30] J.A. Hrabie, L.K. Keefer, Chemistry of the nitric oxide-releasing diazeniumdiolate ("nitrosohydrox ylamine") functional group and its oxygen-substituted derivatives, Chem. Rev. 102 (2002) 1135–1154, https://doi.org/10.1021/cr000028t.
[31] N.W. Rajapakse, D.L. Mattson, Role of L-arginine in nitric oxide production in health and hypertension, Clin. Exp. Pharmacol. 36 (2009) 249–255, https://doi.org/10.1111/j.1440-1681.2008.05123.x.
[32] D.J. Steuhr, Enzymes of the L-arginine to nitric oxide pathway, J. Nutr. 134 (2004) 2748S–2751S, https://doi.org/10.1093/jn/134.10.2748S.
[33] B. Fermor, S.E. Christensen, I. Youn, J.M. Cernanec, C.M. Davies, J.B. Weinberg, Oxygen, nitric oxide and articular cartilage, Eur. Cells Mater. 13 (2007) 56–65, https://doi.org/10.22203/ecm.v013a06.
[34] E. Aguayo, A. Martinez-Sanchez, B. Fernandez-Lobato, F. Alacid, L-citrulline: a non-essential amino acid with important roles in human health, Appl. Sci. 11 (2021) 3293, https://doi.org/10.3390/app11073293.
[35] J. Mu, L. He, W. Fan, W. Tang, Z. Wang, C. Jiang, D. Zhang, Y. Liu, H. Deng, J. Zou, O. Jacobson, J. Qu, P. Huang, X. Chen, Cascade reactions catalyzed by planar metal–organic framework hybrid architecture for combined cancer therapy, Small 16 (2020) 2004016, https://doi.org/10.1002/smll.202004016.
[36] C. Du, M. Zhou, F. Jia, L. Ruan, H. Lu, J. Zhang, B. Zhu, X. Liu, J. Chen, Z. Chai, Y. Hu, D-arginine-loaded metal–organic frameworks nanoparticles sensitize osteosarcoma to radiotherapy, Biomaterials 269 (2021), 120642, https://doi.org/10.1016/j.biomaterials.2020.120642.
[37] L. Zhang, S.S. Wan, C.X. Li, L. Xu, H. Cheng, X.Z. Zhang, An adenosine triphosphate-responsive autocatalytic Fenton nanoparticle for tumor ablation with self-supplied H2O2 and acceleration of Fe (III)/Fe (II) conversion, Nano Lett. 18 (2018) 7609–7618, https://doi.org/10.1021/acs.nanolett.8b03178.
[38] Z. Yu, Q. Li, J. Wang, Y. Yu, Y. Wang, Q. Zhou, P. Li, Reactive oxygen species-related nanoparticle toxicity in the biomedical field, Nanoscale Res. Lett. 15 (2020) 1–14, https://doi.org/10.1186/s11671-020-03344-7.
[39] N. Ghosh, A. Das, S. Chaffee, S. Roy, C.K. Sen, Reactive oxygen species, oxidative damage and cell death, in: Immunity and Inflammation in Health and Disease, Elsevier, 2018, pp. 45–55, https://doi.org/10.1016/B978-0-12-805417-8.00004-4.
[40] Z. Amghouz, J.R. García, A. Adawy, A review on the synthesis and current and prospective applications of zirconium and titanium phosphates, Eng 3 (2022) 161–174, https://doi.org/10.3390/eng3010013.
[41] I.A. Lázaro, R.S. Forgan, Application of zirconium MOFs in drug delivery and biomedicine, Coord. Chem. Rev. 380 (2019) 230–259, https://doi.org/10.1016/j.ccr.2018.09.009.
[42] P.M. Usov, B. Huffman, C.C. Epley, M.C. Kessinger, J. Zhu, W.A. Maza, A.J. Morris, Study of electrocatalytic properties of metal–organic framework PCN-223 for the oxygen reduction reaction, ACS Appl. Mater. Interfaces 9 (2017) 33539–33543, https://doi.org/10.1021/acsami.7b01547.
[43] P. Horcajada, T. Chalati, C. Serre, B. Gillet, C. Sebrie, T. Baati, J.F. Eubank, D. Heurtaux, P. Clayette, C. Kreuz, Porous metal–organic-framework nanoscale carriers as a potential platform for drug delivery and imaging, Nat. Mater. 9 (2010) 172–178, https://doi.org/10.1038/nmat2608.
[44] J. Tejero, A.P. Hunt, J. Santolini, N. Lehnert, D.J. Stuehr, Mechanism and regulation of ferrous heme-nitric oxide (NO) oxidation in NO synthases, J. Biol. Chem. 294 (2019) 7904–7916, https://doi.org/10.1074/jbc.RA119.007810.
[45] M. Mukherjee, A.R. Ray, Nitric oxide synthase-like activity of ion exchange resins modified with iron (III) porphyrins in the oxidation of L-arginine by H2O2: mechanistic insights, Catal. Commun. 8 (2007) 1431–1437, https://doi.org/10.1016/j.catcom.2006.12.010.
[46] X. Wei, R. Dong, D. Wang, T. Zhao, Y. Gao, P. Duffy, X. Zhu, W. Wang, Supramolecular fluorescent nanoparticles constructed via multiple non-covalent interactions for the detection of hydrogen peroxide in cancer cells, Chem. Eur. J. 21 (2015) 11427–11434, https://doi.org/10.1002/chem.201501317.
[47] G. Ravikumar, M. Bagheri, D.K. Saini, H. Chakrapani, A small molecule for theranostic targeting of cancer cells, Chem. Commun. 53 (2017) 13352–13355, https://doi.org/10.1039/C7CC08526E.
[48] J. Hohenberger, K. Ray, K. Meyer, The biology and chemistry of high-valent iron–oxo and iron–nitrido complexes, Nat. Commun. 3 (2012) 1–13, https://doi.org/10.1038/ncomms1718.
[49] H. Maulhardt, S. Verco, M. Baltezor, A. Marin, G. diZerega, Local administration of large surface area microparticle docetaxel to solid carcinomas induces direct cytotoxicity and immune-mediated tumoricidal effects: preclinical and clinical studies, Drug Deliv Transl. Res. (2022) 1–17, https://doi.org/10.1007/s13346-022-01226-2.
[50] K.M. Garland, S. Sevimli, K.V. Kilchrist, C.L. Duvall, R.S. Cook, J.T. Wilson, Microparticle depots for controlled and sustained release of endosomolytic nanoparticles, Cell. Mol. Bioeng. 12 (2019) 429–442, https://doi.org/10.1007/s12195-019-00571-6.
[51] D. Feng, Z.Y. Gu, Y.P. Chen, J.H. Park, Z. Wei, Y. Sun, M. Bosch, S. Yuan, H. C. Zhou, A highly stable porphyrinic zirconium metal–organic framework with shp-a topology, J. Am. Chem. Soc. 136 (2014) 17714–17717, https://doi.org/10.1021/ja510525s.
[52] F.B. Vicente, G. Vespa, A. Miller, S. Haymond, Quantification of arginine and its methylated derivatives in plasma by high-performance liquid chromatography tandem mass spectrometry (LC-MS/MS), Clin. Appl. Mass Spectrom. Biomol. Anal. (2016) 21–30, https://doi.org/10.1007/978-1-4939-3182-8_3.
[53] A. Martínez-Chávez, H. Rosing, C. Gan, Y. Wang, A.H. Schinkel, J.H. Beijnen, Bioanalytical method for the simultaneous quantification of irinotecan and its active metabolite SN-38 in mouse plasma and tissue homogenates using HPLC-fluorescence, J. Chromatogr. B 1149 (2020), 122177, https://doi.org/10.1016/j.jchromb.2020.122177.
[54] H. Li, C.J. Meininger, G. Wu, Rapid determination of nitrite by reversed-phase high-performance liquid chromatography with fluorescence detection, J. Chromatogr. B Biomed. Appl. 746 (2000) 199–207, https://doi.org/10.1016/S0378-4347(00)00328-5.
[55] J. Hu, H. Yang, J. Mu, T. Lu, J. Peng, X. Deng, Z. Kong, S. Bao, X. Cao, J. Zuo, Nitric oxide regulates protein methylation during stress responses in plants, Mole. Cell 67 (2017) 702–710, https://doi.org/10.1016/j.molcel.2017.06.031.
[56] C. Orellana-Tavra, S.A. Mercado, D. Fairen-Jimenez, Endocytosis mechanism of nano metal-organic frameworks for drug delivery, Adv. Healthc. Mater. 5 (2016) 2261–2270, https://doi.org/10.1002/adhm.201600296.
[57] M. Javadi, W.G. Pitt, C.M. Tracy, J.R. Barrow, B.M. Willardson, J.M. Hartley, N. H. Tsosie, Ultrasonic gene and drug delivery using eLiposomes, J. Control. Release 167 (2013) 92–100, https://doi.org/10.1016/j.jconrel.2013.01.009.
[58] S.-N. Kim, C.G. Park, B.K. Huh, S.H. Lee, C.H. Min, Y.Y. Lee, Y.K. Kim, K.H. Park, Y. B. Choy, Metal-organic frameworks, NH2-MIL-88 (Fe), as carriers for ophthalmic delivery of brimonidine, Acta Biomater. 79 (2018) 344–353, https://doi.org/10.1016/j.actbio.2018.08.023.
[59] M.F. Chung, H.Y. Liu, K.J. Lin, W.T. Chia, H.W. Sung, A pH-responsive carrier system that generates NO bubbles to trigger drug release and reverse P-glycoprotein-mediated multidrug resistance, Angew. Chem. - Int. Ed. 54 (2015) 9890–9893, https://doi.org/10.1002/anie.201504444.
[60] J. Li, A. Dirisala, Z. Ge, Y. Wang, W. Yin, W. Ke, K. Toh, J. Xie, Y. Matsumoto, Y. Anraku, Therapeutic vesicular nanoreactors with tumor-specific activation and self-destruction for synergistic tumor ablation, Angew. Chem. 129 (2017) 14213–14218, https://doi.org/10.1002/anie.201706964.
[61] Z.-H. Deng, G.-J. Xu, X.-L. Wang, X. Wang, M.-L. Wang, J.-M. Lin, R.-S. Zhao, A zr (IV)-based porphyrinic metal-organic framework as a solid-phase sorbent for extraction of sulfonamides prior to their quantitation by LC-MS, Microchim. Acta 185 (2018) 1–8, https://doi.org/10.1007/s00604-018-2985-1.
[62] A. Roda, F. Santos, Y.Z. Chua, A. Kumar, H.T. Do, A. Paiva, A.R.C. Duarte, C. Held, Unravelling the nature of citric acid: L-arginine: water mixtures: the bifunctional role of water, Phys. Chem. Chem. Phys. 23 (2021) 1706–1717, https://doi.org/10.1039/D0CP04992A.
[63] J.J. Senkevich, C.J. Mitchell, A. Vijayaraghavan, E.V. Barnat, J.F. McDonald, T.-M. Lu, Unique structure/properties of chemical vapor deposited parylene E, J. Vac. Sci. Technol. A 20 (2002) 1445–1449, https://doi.org/10.1116/1.1487870.
[64] M. Reinmuth, C. Neuhäuser, P. Walter, M. Enders, E. Kaifer, H.J. Himmel, The flexible coordination modes of guanidine ligands in Zn alkyl and halide complexes: chances for catalysis, Eur. J. Inorg. Chem. 1 (2011) 83–90, https://doi.org/10.1002/ejic.201000775.
[65] A. Wojciechowska, A. Gągor, W. Zierkiewicz, A. Jarząb, A. Dylong, M. Duczmal, Metal–organic framework in an l-arginine copper (ii) ion polymer: structure, properties, theoretical studies and microbiological activity, RSC Adv. 5 (2015) 36295–36306, https://doi.org/10.1039/C5RA02790J.
[66] J.-E. Kim, Y.-J. Park, Hyaluronan self-agglomerating nanoparticles for non-small cell lung cancer targeting, Cancer Nanotechnol. 13 (2022) 1–24, https://doi.org/10.1186/s12645-022-00115-0.
[67] Y. Kato, S. Ozawa, C. Miyamoto, Y. Maehata, A. Suzuki, T. Maeda, Y. Baba, Acidic extracellular microenvironment and cancer, Cancer Cell Int. 13 (2013) 1–8, https://doi.org/10.1186/1475-2867-13-89.
[68] C.R. Justus, L. Dong, L.V. Yang, Acidic tumor microenvironment and pH-sensing G protein-coupled receptors, Front. Physiol. 4 (2013) 354, https://doi.org/10.3389/fphys.2013.00354.
[69] N.Y. Chun, S.-N. Kim, Y.S. Choi, Y.B. Choy, PCN-223 as a drug carrier for potential treatment of colorectal cancer, J. Ind. Eng. Chem. 84 (2020) 290–296, https://doi.org/10.1016/j.jiec.2020.01.010.

[70] W. Lin, Q. Hu, K. Jiang, Y. Yang, Y. Yang, Y. Cui, G. Qian, A porphyrin-based metal–organic framework as a pH-responsive drug carrier, J. Solid State Chem. 237 (2016) 307–312, https://doi.org/10.1016/j.jssc.2016.02.040.
[71] P. Ebrahimnejad, R. Dinarvand, A. Sajadi, M.R. Jaafari, A.R. Nomani, E. Azizi, M. Rad-Malekshahi, F. Atyabi, Preparation and in vitro evaluation of actively targetable nanoparticles for SN-38 delivery against HT-29 cell lines, Nanomed. Nanotechnol. Biol. Med. 6 (2010) 478–485, https://doi.org/10.1016/j.nano.2009.10.003.
[72] M.J. Abualreish, A. Noubigh, Experimental measurement and correlation of two α-amino acids solubility in aqueous salts solutions from 298.15 to 323.15 K, Korean Chem. Eng. Res. 58 (2020) 98–105, https://doi.org/10.9713/kcer.2020.58.1.98.
[73] Y. Wu, T. Guo, Y. Qiu, Y. Lin, Y. Yao, W. Lian, L. Lin, J. Song, H. Yang, An inorganic prodrug, tellurium nanowires with enhanced ROS generation and GSH depletion for selective cancer therapy, Chem. Sci. 10 (2019) 7068–7075, https://doi.org/10.1039/c9sc01070j.
[74] Y. Tang, Y. Ji, C. Yi, D. Cheng, B. Wang, Y. Fu, Y. Xu, X. Qian, Y.E. Choonara, V. Pillay, Self-accelerating H2O2-responsive plasmonic nanovesicles for synergistic chemo/starving therapy of tumors, Theranostics 10 (19) (2020) 8691, https://doi.org/10.7150/thno.45392.
[75] R. Guo, Y. Tian, Y. Wang, W. Yang, Near-infrared laser-triggered nitric oxide nanogenerators for the reversal of multidrug resistance in cancer, Adv. Funct. Mater. 27 (2017) 1606398, https://doi.org/10.1002/adfm.201606398.
[76] C. Orellana-Tavra, E.F. Baxter, T. Tian, T.D. Bennett, N.K. Slater, A.K. Cheetham, D. Fairen-Jimenez, Amorphous metal–organic frameworks for drug delivery, Chem. Commun. 51 (2015) 13878–13881, https://doi.org/10.1039/C5CC05237H.
[77] A. Sadhu, Y. Moriyasu, K. Acharya, M. Bandyopadhyay, Nitric oxide and ROS mediate autophagy and regulate Alternaria alternata toxin-induced cell death in tobacco BY-2 cells, Sci. Rep. 9 (2019) 1–14, https://doi.org/10.1038/s41598-019-45470-y.
[78] H.-C. Zhang, F. Zhang, B. Wu, J.-H. Han, W. Ji, Y. Zhou, R.-F. Niu, Identification of the interaction between P-glycoprotein and Anxa2 in multidrug-resistant human breast cancer cells, Cancer Biol. Med. 9 (2012) 99, https://doi.org/10.3969/j.issn.2095-3941.2012.02.003.
[79] Y. Yang, N. Wu, Z. Wang, F. Zhang, R. Tian, W. Ji, X. Ren, R. Niu, Rack1 mediates the interaction of P-glycoprotein with Anxa2 and regulates migration and invasion of multidrug-resistant breast cancer cells, Int. J. Mol. Sci. 17 (2016) 1718, https://doi.org/10.3390/ijms17101718.
[80] A.W. Carpenter, M.H. Schoenfisch, Nitric oxide release: part II. Therapeutic applications, Chem. Soc. Rev. 41 (2012) 3742–3752, https://doi.org/10.1039/c2cs15273h.
[81] A. McKinlay, J. Eubank, S. Wuttke, B. Xiao, P. Wheatley, P. Bazin, J.-C. Lavalley, M. Daturi, A. Vimont, G. De Weireld, Nitric oxide adsorption and delivery in flexible MIL-88 (Fe) metal–organic frameworks, Chem. Mater. 25 (2013) 1592–1599, https://doi.org/10.1021/cm304037x.
[82] A.C. McKinlay, B. Xiao, D.S. Wragg, P.S. Wheatley, I.L. Megson, R.E. Morris, Exceptional behavior over the whole adsorption− storage− delivery cycle for NO in porous metal organic frameworks, J. Am. Chem. Soc. 130 (2008) 10440–10444, https://doi.org/10.1021/ja801997r.
[83] J.F. Eubank, P.S. Wheatley, G. Lebars, A.C. McKinlay, H. Leclerc, P. Horcajada, M. Daturi, A. Vimont, R.E. Morris, C. Serre, Porous, rigid metal (III)-carboxylate metal-organic frameworks for the delivery of nitric oxide, APL Mater. 2 (2014), 124112, https://doi.org/10.1063/1.4904069.
[84] J.L. Harding, M.M. Reynolds, Composite materials with embedded metal organic framework catalysts for nitric oxide release from bioavailable S-nitrosothiols, J. Mater. Chem. B 2 (2014) 2530–2536, https://doi.org/10.1039/C3TB21458C.
[85] X. Zhang, Y. Wang, J. Liu, J. Shi, D. Mao, A.C. Midgley, X. Leng, D. Kong, Z. Wang, B. Liu, A metal-organic-framework incorporated vascular graft for sustained nitric oxide generation and long-term vascular patency, Chem. Eng. J. 421 (2021), 129577, https://doi.org/10.1016/j.cej.2021.129577.
[86] M.J. Neufeld, A. Lutzke, W.M. Jones, M.M. Reynolds, Nitric oxide generation from endogenous substrates using metal–organic frameworks: inclusion within poly (vinyl alcohol) membranes to investigate reactivity and therapeutic potential, ACS Appl. Mater. Interfaces 9 (2017) 35628–35641, https://doi.org/10.1021/acsami.7b11846.
[87] Z. Liu, T. Li, F. Han, Y. Wang, Y. Gan, J. Shi, T. Wang, M.L. Akhtar, Y. Li, A cascade-reaction enabled synergistic cancer starvation/ROS-mediated/chemo-therapy with an enzyme modified Fe-based MOF, Biomater Sci. 7 (2019) 3683–3692, https://doi.org/10.1039/C9BM00641A.
[88] B. Meunier, J. Bernadou, Metal-oxo species in P450 enzymes and biomimetic models. Oxo-hydroxo tautomerism with water-soluble metalloporphyrins, Top. Catal. 21 (2002) 47–54, https://doi.org/10.1023/A:1020599814238.
[89] A. Sukhanova, S. Bozrova, P. Sokolov, M. Berestovoy, A. Karaulov, I. Nabiev, Dependence of nanoparticle toxicity on their physical and chemical properties, Nanoscale Res. Lett. 13 (2018) 1–21, https://doi.org/10.1186/s11671-018-2457-x.
[90] Y. He, K. Park, Effects of the microparticle shape on cellular uptake, Mol. Pharm. 13 (2016) 2164–2171, https://doi.org/10.1021/acs.molpharmaceut.5b00992.
[91] J. Chen, Y. Zhu, S. Kaskel, Porphyrin-based metal-organic frameworks for biomedical applications, Angew. Chem. Int. Ed. 60 (2021) 5010–5035, https://doi.org/10.1002/anie.201909880.